2024 IEEE International Symposium on Antennas and Propagation and INC/USNC-URSI Radio Science Meeting (AP-S/INC-USNC-URSI) | 979-8-3503-6990-8/24/$31.00 ©2024 IEEE | DOI: 10.1109/AP-S/INC-USNC-URSI52054.2024.10686667

Single-bit mmWave Reconfigurable Intelligent Surface with Suppressed Quantization Lobe

Aditya S. Shekhawat and Georgios C. Trichopoulos
School of Electrical, Computer, and Energy Engineering, Arizona State University, Tempe, Arizona, USA
(aditya.shekhawat, gtrichop)asu.edu

***Abstract*—We introduce a millimeter wave (mmWave) single-bit reconfigurable intelligent surface (RIS) that allows electronic beamsteering with no quantization lobes. Incorporating an optimized random fixed phase delay pattern across the aperture, we manage to suppress radiation artifacts stemming from quantization errors. Additionally, the RIS design employs a modular approach by using PCB compatible 2.5D packaging. As such, the radiating elements, phase shifters, delay lines, interconnects, and necessary shift registers are integrated within a tile that can be laterally cascaded and form arbitrarily large RISs. We present the RCS measurement results of a 4-tile prototype (1,024-unit cells) with electronic beam-steering up to ±60 degrees, with more than 10 dB quantization lobe suppression at a center frequency of 27.2 GHz.**

I. Introduction

5G and future generations of wireless communication technologies utilize millimeter-wave (mmWave) frequencies to enhance data rates and expand broadband access. However, mmWave signals face significant coverage challenges due to the short propagation range and vulnerability to absorption and scattering, leading to a low signal-to-noise (SNR) ratio or no coverage. Densifying base station networks can improve coverage but is costly due to high hardware, installation, and maintenance costs. Alternatively, reconfigurable intelligent surfaces (RISs) [1]-[2] can provide a more efficient solution in boosting mmWave signal propagation. An RIS consists of low-cost passive metasurfaces (no RF gain) that allow the redirection of stray mmWaves toward desirable directions. Strategically positioned RISs in a wireless network can create additional propagation paths to non-line-of-sights (NLoS) areas, improving signal coverage and SNR.

In a dynamic wireless communication environment, electronic beam control is vital and can be achieved by integrating the RIS's radiating elements with continuous or discreet (digital) phase shifters, such as RF PIN diodes, MEMs, and varactors. Although beamforming is favored by fine phase modulation, the control circuity becomes complex and/or bulky with the associated multi-bit phase shifter control. This problem is further exacerbated at mmWave frequencies, where the unit cells become smaller and the aperture electrically larger (more unit cells). Furthermore, multi-bit phase modulation can result in higher power consumption, more signal overhead from the associated microcontroller units (MCUs), and slower beam-steering speed. Therefore, the 1-bit quantization is favored due to its simplicity, although it has its own challenges, such as the

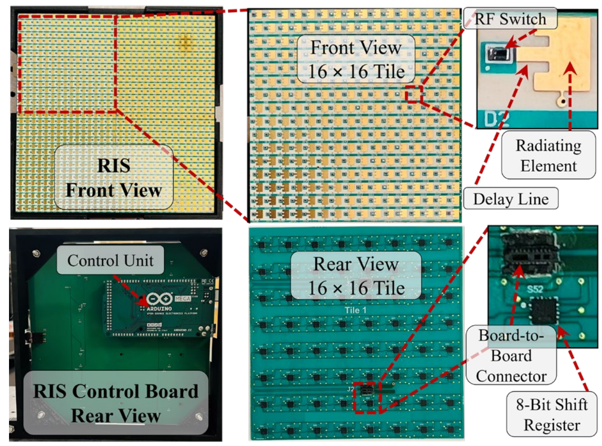

Fig. 1. mmWave RIS prototype consisting of four 16×16 1-bit RIS tiles (left), the control board (left), and details about the unit cell (right) design.

quantization lobes. To overcome this, a compact 1-bit unit cell design using a random pre-phasing technique was introduced in [3], albeit for fixed beam reflective metasurfaces. Here, we present for the first time the design of a scalable, tiled-RIS design with quantization lobe suppression using a single-bit phase. The proposed tile topology can pave the way for realizing larger apertures for higher gain and narrower beamwidths. In this paper, we briefly discuss the RIS element design, describe the measurement setup, and present the electronic beamsteering results for a wide range of scanning angles.

II. RIS Element Design

Employing the phase randomization approach detailed in [3], the phase profile of an M × N array can be effectively altered. This is achieved by introducing random yet consistent phase delays, denoted as Φ_{mn}^{rand}, to each unit cell, such that the continuous excitation phase of each element obtained as:

$$\Phi_{mn} = \Phi_{mn}^{\text{ele}} - \Phi_{mn}^{illum} - \Phi_{mn}^{rand} \tag{1}$$

For 1-bit quantization, the required continuous excitation phase of each element to steer the beam in the desired direction, which is a combination of the element phase (Φ_{mn}^{ele}) for beam direction, the phase of the incoming wave (Φ_{mn}^{illum}), and random phase Φ_{mn}^{rand} is rounded off to 0° and 180° phase values. To design an RIS with the random pre-phasing technique, a four-layer stack-up for unit cells is used. The top layer hosts various components, such as a microstrip patch (radiating element), a PIN diode (MACOM MA4AGP907),

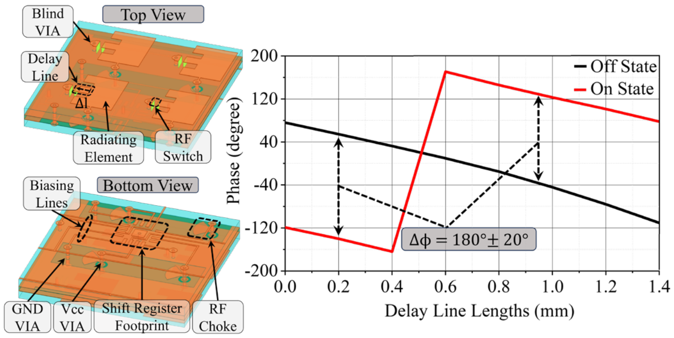

Figure 2. RIS super-cell design (a) 3D top and bottom view, depicting various layers, RF elements, and footprints for DC components; (b) Simulation results: reflection phase vs delay line lengths for ON and OFF state.

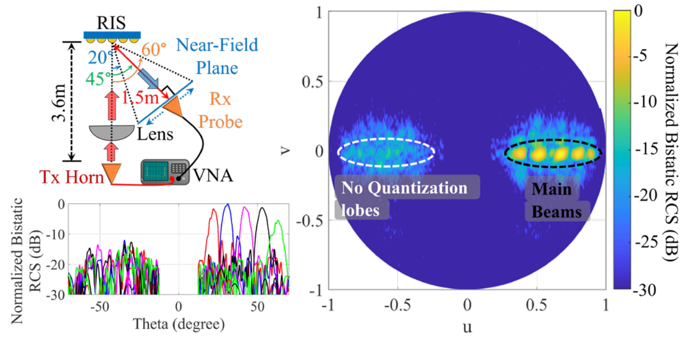

Figure 3. Measurement setup (top left) used to characterize beamsteering of the proposed mmWave RIS, measured 2D (bottom left) and 3D (right) RCS pattern for various steering angles. The patterns were measured for normal incidence θ_i = 0° and reflection angles θ_d = 20°, 30°, 40°, 50°, and 60°.

and an inset feed (delay line). The second layer serves as a common ground plane (RF/DC), while the third layer is a Vcc plane with rectangular slots to employ an RF choke (λ/4 radial stub). The bottom layer accommodates biasing components, such as shift registers (TI SN74HC595B) and connectors for vertical board assembly. Shift registers are strategically placed between a group of 2 × 2 unit cells (super-cell), as depicted in Fig. 2, to control the states of four switches by supplying the desired current. This super-cell topology repeats across the aperture of the RIS, allowing independent control of every RF switch.

The electromagnetic analysis is carried out in ANSYS Electronics Desktop to evaluate the super-cell performance. Using periodic boundary conditions analysis, a Floquet port is used to excite the super-cell and to account for the coupling between the elements. The super-cell is evaluated for two states: first, when all four PIN diodes are ON, state 1 (180°), and second, when they are OFF, state 2 (0°). The reflection phase in both states is optimized by adjusting the radiating element and feed dimensions to achieve a 180°±20° phase difference, as illustrated in Fig. 2. The RF switch imperfections are accounted for by incorporating the PIN diode's measured *S*-parameters provided by the vendor for both biasing (ON/OFF) conditions. Additionally, we vary the inset feed length (Δl) for every radiating element to create random phase delays for each unit cell within the 0°-180° range. This variation in delay line length, from 0 mm to 1.4 mm, maintains the necessary phase difference and provides random phases, as demonstrated in Fig. 2.

Further, the performance of the finite array is evaluated and can achieve beam-steering in ±60° in both azimuth and elevation planes. The center frequency of operation is 27.2 GHz with a 3-dB maximum RCS bandwidth of 2 GHz.

III. RIS Fabrication and Characterization

A. Measurement setup:

We use a near-field measurement setup to assess the bistatic radar cross section (RCS) of the RIS prototype. To emulate the far-field conditions anticipated in real-world wireless communication environments, where the RIS would be illuminated by a plane wave, we employ a quasi-optical setup with a large aperture objective lens. This arrangement generates a wide collimated beam, effectively mimicking a plane wave impinging on the RIS aperture. The transmitting and receiving antennas are connected to the respective ports of a vector network analyzer (VNA), and the measured coupled signal (S_{21}), which is proportional to the RCS of the RIS, is recorded. The receiving probe gathers data on a planar near-field along a rectangular x-y grid and is rotated radially at 45° to avoid blocking the transmitted signal, which limits the scan range to approximately [20°, 60°]. Finally, we employ near-field to far-field transformation technique to derive the far-field 3D RCS patterns at various reflection angles.

B. Measured Radar Cross Section:

The measured RCS patterns of the RIS at 27.2 GHz are shown in Fig. 3. As expected, only a single main lobe appears per beam at +20°, +30°, +40°, +50°, and +60° while the quantization lobe at -20°, -30°, -40°, -50°, and -60° respectively is suppressed due to implementation of the random phases in the feed network of the RIS unit cells. From the measurements, it can be observed that the quantization lobe is suppressed by more than 10 dB.

IV. Conclusion

We presented a modular and scalable RIS design approach based on 16 × 16 element tiles operating at mmWave frequencies. The measured RCS results of the RIS tiles demonstrated a single main lobe with more than 10dB suppression of the quantization lobe at various reflection angles. Also, a 3-dB bandwidth of 7.4% and a half-power beamwidth of 4°, 4.3°, 4.5°, 4.8°, and 5° are obtained for 20°, 30°, 40°, 50°, and 60° reflection angles respectively. Furthermore, the proposed topology is power-efficient and can be extended to designs operating at higher mmWave frequencies and support dual polarization designs or 2-bit phase shifting, enhancing the design's feasibility.

References

[1] B.M. H. Dahri, M. H. Jamaluddin, M. I. Abbasi, and M. R. Kamarudin, "A review of wideband reflectarray antennas for 5G communication system," IEEE Access, vol. 5, pp. 17803-17815, 2017.

[2] V. Jamali, A. M. Tulino, G. Fischer, R. Muller, and R. Schober, "Scalable and energy-efficient millimeter massive MIMO architecture: Reflect-array and transmit-array antennas," in proc. IEEE Int. Conf. Commun. (ICC), Shanghai, China, 2019, pp. 1-7.

[3] B. G. Kashyap, P. C. Theofanopoulos, Y. Cui and G. C. Trichopoulos, "Mitigating Quantization Lobes in mmWave Low-Bit Reconfigurable Reflective Surfaces," in *IEEE Open Journal of Antennas and Propagation*, vol. 1, pp. 604-614, 2020.